International Journal of Biological Macromolecules 248 (2023) 125835

Contents lists available at ScienceDirect

International Journal of Biological Macromolecules

journal homepage: www.elsevier.com/locate/ijbiomac

# 3D printed Styrax Liquidus (*Liquidambar orientalis* Miller)-loaded poly (L-lactic acid)/chitosan based wound dressing material: Fabrication, characterization, and biocompatibility results

Hanife Yuksel Cakmak [a], Hasan Ege [b,c], Senanur Yilmaz [b,d], Gokhan Agturk [c,e], Fulya Dal Yontem [f,g], Gozde Enguven [b,d], Abdurrahman Sarmis [h], Zeren Cakmak [a], Oguzhan Gunduz [b,d], Zeynep Ruya Ege [b,i,*]

[a] *Kartal Prof. Dr. Saban Teoman Durali Science and Art Center, Istanbul, Turkey*
[b] *Center for Nanotechnology and Biomaterials Applied and Research, Marmara University, Istanbul, Turkey*
[c] *Institute of Health Sciences, Department of Physiology, Istanbul University-Cerrahpasa, Istanbul, Turkey*
[d] *Department of Metallurgical and Materials Engineering, Faculty of Technology, Marmara University, Istanbul, Turkey*
[e] *Department of Physiology, School of Medicine, Halic University, Istanbul, Turkey*
[f] *Department of Biophysics, Koc University School of Medicine, Koç University, Sariyer, Istanbul, Turkey*
[g] *Koc University Research Center for Translational Medicine (KUTTAM), Sariyer, 34450 Istanbul, Turkey*
[h] *Department of Medical Microbiology Laboratory, Goztepe Prof. Dr. Suleyman Yalcin City Hospital, Istanbul, Turkey*
[i] *Department of Biomedical Engineering, Faculty of Engineering and Architecture, Istanbul Arel University, Istanbul, Turkey*

ARTICLE INFO

*Keywords:*
3D printing
Wound dressing
Wound healing
Tissue engineering
Styrax liquidus
Controlled releasing

ABSTRACT

The medicinal plant of Styrax liquidus (ST) (sweet gum balsam) which extracted from *Liquidambar orientalis* Mill tree, was loaded into the 3D printed polylactic acid (PLA)/chitosan (CS) based 3D printed scaffolds to investigate its wound healing and closure effect, in this study. The morphological and chemical properties of the ST loaded 3D printed scaffolds with different concentrations (1 %, 2 %, and 3 % wt) were investigated by Scanning Electron Microscopy (SEM) and Fourier Transform Infrared Spectroscopy (FT-IR), respectively. In addition, the mechanical and thermal properties of the materials were investigated by Tensile test and Differential Scanning Calorimetry (DSC), respectively. The antimicrobial activities of the ST loaded 3D printed scaffolds and their incubation media in the PBS (pH 7.4, at 37 °C for 24 h) were investigated on two Gram-positive and two Gram-negative standard pathogenic bacteria with the agar disc diffusion method. The colorimetric MTT assay was used to determine the cell viability of human fibroblast cells (CCD-1072Sk) incubated with free ST, ST loaded, and unloaded 3D printed scaffolds. The 1 % and 2 % (wt) ST loaded PLA/CS/ST 3D printed scaffolds showed an increase in the cell number. Annexin V/PI double stain assay was performed to test whether early or late apoptosis was induced in the PLA/CS/1 % ST and PLA/CS/2 % ST loaded groups and the results were consistent with the MTT assay. Furthermore, a wound healing assay was carried out to investigate the effect of ST loaded 3D printed scaffolds on wound healing in CCD-1072Sk cells. The highest wound closure compared to the control group was observed on cells treated with PLA/CS/1 % ST for 72 h. According to the results, novel biocompatible ST loaded 3D printed scaffolds with antimicrobial effect can be used as wound healing material for potential tissue engineering applications.

## 1. Introduction

The wound healing and tissue repair process consists of sequential interrelated stages, called inflammatory, proliferative, and remodeling, at the molecular and cellular levels [1]. In acute wounds, the wound healing process is rapid and depends on the proper progression of these stages. Chronic wounds, unlike acute wounds, do not exhibit a proper wound healing process, causing a delay in healing time and this leads to a decrease in individual life quality along with an increased financial burden [2]. The treatment of wounds requires surgical operations,

* Corresponding author at: Department of Biomedical Engineering, Faculty of Engineering and Architecture, Istanbul Arel University, Istanbul, Turkey.
*E-mail address:* zeynepruyaege@arel.edu.tr (Z.R. Ege).

https://doi.org/10.1016/j.ijbiomac.2023.125835
Received 19 March 2023; Received in revised form 26 June 2023; Accepted 12 July 2023
Available online 18 July 2023

debridement (removal of dead/inflamed tissue), or applying wound dressing materials [3].

Commercially available traditional wound dressing materials, including gauze, natural/synthetic bandages or lint have some disadvantages because they couldn't provide a moist environment for better wound healing, and thus they are required frequent change [4]. These limitations have created the necessity for new strategies for better wound management.

In recent years, polymeric hydrogel based 3D printed wound dressing materials have drawn attention due to their superior properties such as creating a three-dimensional extracellular matrix (ECM) like moist environment for the cells where they can migrate and proliferate, allowing oxygen penetration through porous structure, and inducing wound healing process along with cell attachment [5]. In the literature, effective dressing materials have been successfully produced by using different combinations of natural/synthetic polymer composites in the 3D printing system for the development of wound dressings with biocompatible and biodegradable properties [6]. Besides, it is possible to incorporate biologically active agents (drugs, plant extracts, nanoparticles) during the 3D fabrication process of wound dressing material. This enables the controlled and sustained release of bioactive agents at the wound site as locally [7].

Chitosan (CS), a derivative of chitin, is commonly used with other polymers due to its desired biological properties, such as biocompatibility, biodegradability, low toxicity, homeostatic function, pain relief, and antimicrobial activity [8]. CS provides a non-protein matrix for 3D tissue growth and activates macrophages. CS based hydrogels could stimulate fibroblast proliferation, angiogenesis, regular collagen deposition, and increase the level of natural hyaluronic acid (HA) synthesis at the wound site [9]. Owing to these properties of CS, it can be used as a copolymer with polylactic acid (PLA) to enhance the biological activity in the wound environment and to fabricate biologically active wound dressing material.

PLA is one of the Food and Drug Administration **(**FDA) approved biomaterials, with non-immunogenic, biocompatible, biodegradable, and high mechanical properties [10,11]. Domínguez-Robles et al. reported 3D printed PLA and lignin composite material that can be used in wound dressing applications due to its antioxidant effect [12]. Calamak-Ermis fabricated 3D printed Ag functionalized PLA based composite material, which has the potential to be used in wound healing applications [13].

Styrax Liquidus (ST) is a resinous exudate extracted from the wounded bark (in the form of balsam) of the *Liquidambar orientalis* Miller tree, grown in the eastern Mediterranean region of Turkey. ST has been used since ancient times, particularly in Turkish folk medicine for the treatment of various health complications such as wounds, burns, and peptic ulcers [14].

In this study, ST loaded PLA/CS based composite 3D printed scaffolds for wound dressing application were fabricated by 3D printing technology. With this study, the incorporation of ST into 3D printed scaffolds and its controlled release from the scaffolds are reported for the first time in the literature.

In the literature, several studies have reported that either free ST or encapsulated ST have antibacterial and antioxidant activities. [15,16]. Demir et al. investigated the antibacterial and antioxidant effects of ST incorporated Poly (ε-caprolactone) (PCL) electrospun composite nanofibers for wound dressing application. The results of the study showed that the effective biological activity of ST depends on its weight ratio. The different weight ratios of ST (25, 50, and 100 %, wt) were loaded to the hybrid nanofibers based on the PCL polymer weight by electrospinning method. In their study, PCL/ST nanofibers loaded with 100 % (wt) ST have shown better cell viability with mouse embryonic fibroblast (MEF) cells. Besides, cytotoxicity analysis of ST on MEF cells revealed that fibrous scaffolds increased cell number with high viability [17]. Contrastly, in this study, high cytotoxicity was observed in human fibroblast cells when the loaded ST ratio exceeds even 2 % (wt) in the 3D printed scaffolds. In addition, 3D printed PLA/CS based scaffolds loaded with 5, 10, and 15 % (wt) ST were also produced which showed high cell toxicities in the human fibroblast cell line (Fig. S1).

The antimicrobial activities of the ST loaded 3D printed scaffolds and their incubation mediums were investigated on two Gram-positive and two Gram-negative standard pathogenic bacteria (*Staphylococcus aureus* ATCC 29213, *Enterococcus faecalis* ATCC 29212, *Escherichia coli* ATCC 25922, *Pseudomonas aeruginosa* ATCC 27853) with the agar disc diffusion method. The incubation medium of ST loaded 3D printed scaffolds and free ST has shown an excellent antibacterial effect against *S. aureus*. This result could give an idea for new research to prevent infections caused by colonized *S. aureus* in the wound area.

Therefore, the results of the study demonstrated that the delayed wound healing process caused by infection can be prevented due to the antimicrobial effect of ST. In addition, the high wound closure tendency obtained in the wound closure tests performed with 1 % (wt) ST loaded scaffolds in human fibroblast cells reveals that these wound dressings are the best candidate for the fast wound healing process.

## 2. Materials and methods

### 2.1. Materials

Poly (L-lactic acid) (PLA) 2003D (good biocompatibility for cells [18]) was obtained from Nature Works LLC, Minnetonka, MN. Low molecular weight chitosan (CS, low molecular weight,) was purchased from Sigma-Aldrich (St. Louis, USA). Chloroform (CAS: 67-66-3) and acetic acid (CH3COOH) were obtained from Sigma-Aldrich. Human fibroblast cells (CCD-1072Sk) were purchased from American Type Culture Collection (ATCC) for cell culture studies. DMEM (Dulbecco's Modified Eagle Medium), %10 FBS (fetal bovine serum), penicillin/streptomycin, BSA (bovine serum albumin), and phosphate buffer saline (PBS) were purchased from Thermo Fisher Scientific (Massachusetts, USA).

Ethanol (99 % purity, vol./vol.), (3-(4,5-dimethyl-2-thiazol)-2,5-diphenyl-2H-tetrazolium bromide) MTT, Trypsin/EDTA solution at 0.25 % (w./v.), Triton X-100, paraformaldehyde, and hexamethyldisilazane (HMDS) (99 % purity, vol./vol.) were purchased from Sigma-Aldrich (St. Louis, USA).

### 2.2. Preparation of Styrax Liquidus (Liquidambar orientalis Miller) oil

Styrax Liquidus (ST) is obtained from the wounded bark of the *Liquidambar orientalis* Miller tree (Hamamelidaceae family), which is known as the sweetgum tree and widely found in the Mugla region of Turkey. To convert it to balsam form, ST is processed by boiling and pressing. It has a brownish color, a paste-like texture, and a unique aroma. ST was purchased from a local herbalist in Mugla-Koycegiz.

### 2.3. Preparation of the 3D printing solutions

Firstly, PLA and CS solutions were prepared separately. 15 % (*w/v*) PLA was dissolved in chloroform and 2 % (w/v) CS was dissolved in 90 % acetic acid, then put on the magnetic stirrer overnight. After complete dissolution was achieved, PLA and CS were mixed in a volume ratio of 2:1, respectively. The different concentrations of ST (1 %, %2, and 3 % wt) were prepared by adding them to PLA/CS mixed solution. All processes were done at room temperature (23 °C).

### 2.4. Fabrication of the 3D printed scaffolds

The scaffold configuration was designed in a square shape with 20 mm × 20 mm × 1 mm dimensions and 7 layers using the Solidworks program and converted to G-codes by Simplify3d software. In the fabrication of composite scaffolds, an extrusion-based 3D printer (Hyrel 3D, SDS-5 Extruder, GA, USA) was used. A polymer solution, containing

PLA and CS, was placed into a 10 ml syringe which is connected to the 28 Ga needle tip.

In order to obtain an ideal pore shapes and non collapse printed strips, following printing parameters were optimized as: the printing rate = 10 mm/s, the flow rate = 1 ml/h, the infill density = 96 %, the total layer = 7, and the infill pattern was rectilinear.

Fig. 1 schematically represents the 3D printing of ST loaded PLA/CS based composite scaffold.

### 2.5. Characterization of the chemical and physical properties of 3D printed scaffolds

#### 2.5.1. Rheological analysis of 3D printing solutions

The physical properties of all prepared solutions (viscosity, density, and surface tension) were determined. The solution viscosity was measured at room temperature with a digital viscometer (DV-E, Brookfield AMETEK, USA). To analyze solution density, a standard 10 ml density bottle, DIN ISO 3507-Gay-Lussac (Boru Cam Inc., Republic of Turkey) was used. The surface tension of the solutions was obtained by using a tensiometer (Sigma 703D, Attention, Germany). Each test was repeated three times. Before experiments, all equipment was calibrated.

#### 2.5.2. Scanning electron microscopy (SEM)

The morphological properties and the pore size of 3D printed scaffolds were evaluated by SEM (EVO LS 10, ZEISS, USA). Prior to SEM analysis, the printed scaffolds were coated with gold and palladium for 120 s using a sputter coating machine (Quorum SC7620, USA). The morphological appearance and pore size differences of each scaffold were analyzed by digital image software (Olympus AnalySIS, USA). Thereafter average pore size was determined by the SPSS analysis program.

#### 2.5.3. Fourier transform infrared spectroscopy (FT-IR)

Chemical characterization of each 3D printed scaffold was conducted by FT-IR (Jasco, FT/IR 4700) with the spectra ranging between 4000 and 400 $cm^{-1}$ at 4 $cm^{-1}$ resolution and averaged over 32 scans. Each spectrum was recorded at room temperature. Prior to analysis, ST loaded and unloaded 3D printed scaffolds were cut into small pieces. ST was also analyzed in liquid form to ensure the encapsulation efficiency of the different concentrations of ST (%1, %2, %3 wt) in 3D printed scaffolds.

#### 2.5.4. Differential scanning calorimetry (DSC)

Differential scanning calorimetry (DSC) (Shimadzu, Japan) was used to investigate the thermal properties of the 3D printed scaffolds such as glass transition temperatures ($T_g$) and melting temperature ($T_m$). The 3D printed scaffolds were placed into aluminum pans and DSC was performed in the temperature range from 25 to 300 °C at the scanning rate of 10 °C/min.

#### 2.5.5. Mechanical properties of the scaffolds

The stress/strain curves of the 3D printed scaffolds were obtained by using a tensile test device (SHIMADZU, EZ-LX, CHINA) with a 5 mm/min test speed. Five groups of scaffolds (2 cm × 1,5 cm in size) were analyzed and 2 samples were selected as a subgroup. The thicknesses of the samples were measured by a digital micrometer (Mitutoyo MTI Corp., Aurora, IL).

#### 2.5.6. Swelling and degradation behaviors of scaffolds

The swelling and degradation behaviors of 3D printed scaffolds were examined in phosphate-buffered saline solution (PBS; pH 7.4) at 37 °C and maintained at 250 rpm in the thermal shaker (BIOSAN TS-100) during each time interval (day 1, 3, 5, 7, 14, 21 and 28). The PBS solution was refreshed at each time interval for the maintenance of biological environment activity. 3D printed PLA, PLA/CS, and different concentrations of ST loaded (1 %, 2 %, and 3 % wt) PLA/CS scaffolds were weighed to get the initial weights ($W_0$) of the scaffolds and placed into 1 ml PBS media (pH 7.4) in eppendorf tubes. Two samples were tested for each group for degradation and swelling tests. For the swelling test, each scaffold was removed on days 1, 3, 5, 7, 14, 21, and 28. The removed scaffolds were slightly dried with filter paper before being weighed in the wet condition ($W_w$). The swelling value (S) was calculated by using Eq. (1) [19]:

$$S = (Ww–Wo)/Wo \times 100 \quad (1)$$

For the degradation test, each scaffold was removed on days 1, 3, 5, 7, 14, 21, and 28. The removed scaffolds were washed with deionized water and then dried for 24 h at room temperature (23 °C) and weighed ($W_t$). The degradation value (D) was calculated by using Eq. (2) [19]:

$$D = (W_o - W_t)/W_o \times 100 \quad (2)$$

#### 2.5.7. In vitro ST release and release kinetic assay

To evaluate the release kinetics of ST at different concentrations (1 %, 2 %, and 3 % wt) from 3D printed PLA/CS composite scaffolds, each scaffold was immersed in 1 ml of PBS (pH 7.4) and maintained in a horizontally shaking thermal shaker (BIOSAN TS-100) (at 37 °C, 250 rpm). At defined time intervals (0, 0.25, 0.5, 0.75, 1, 2, 3, 5, 8, 24, 48, 72, 96, 168, 336, 504 h), 1 ml PBS was removed from each sample for UV analysis and 1 ml of fresh PBS was added to all samples to continue the releasing study. The released amount of ST in PBS at each time interval was monitored by measuring the UV absorbance of the maximum peak at 274 nm with a UV–vis spectroscopy (Shimadzu UV-3600 spectrometer). In order to calculate the released amount of ST from scaffolds, the standard calibration curve was constructed with 5 different concentrations (2, 4, 6, 8, and 10 mg/ml) of ST solution which were prepared in ethanol. The samples at all time points were run in triplicate ($n = 3$). The cumulated ST release ratio was calculated with Eq. (3) for each time interval [18].

$$\text{ST release ratio}\% = M_t/M_\infty \times 100 \quad (3)$$

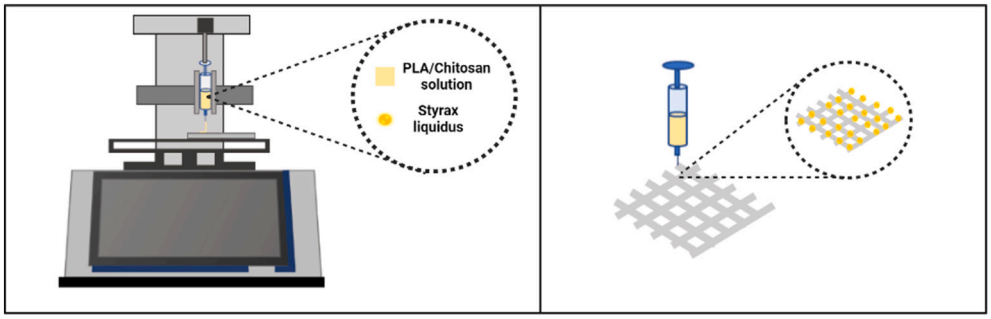


**Fig. 1.** Schematic representation of experimental setup and 3D printed Styrax liquidus-loaded PLA/CS 3D scaffold.

where $M_t$ is the amount of ST released at time t and $M_\infty$ is the total amount of ST added theoretically loaded into the 3D printed scaffolds. In addition, the in vitro release kinetics were evaluated for each concentration of ST.

The kinetics and mechanism of ST release were evaluated for all the 3D printed scaffold formulations by fitting the data to the different kinetic models. All formulations were given in Supporting information (SI).

The encapsulation efficiency (EE %) of ST loaded 3D printed scaffolds was calculated using Eq. (4):

$$EE\ (\%) = D_m/D_t \times 100 \quad (4)$$

where, $D_m$ is the actual amount of ST in the 3D printed PLA/CS scaffolds and $D_t$ is the initial amount of ST used for the fabrication of 3D printed PLA/CS [20,21].

For EE (%) calculation, 3D printed scaffolds were weighed and dissolved completely in their solvent system via vortex mixing. Then, the samples were centrifuged at 600 rpm for 5 min. Then, supernatants were collected and measured for their absorbance by using a UV–visible spectrophotometer (Shimadzu UV-3600, Japan) at 274 nm. All measurements were repeated three times.

### 2.6. Antibacterial assay

The *in vitro* antibacterial activity of free ST and ST loaded (1 %, 2 %, and 3 % wt) 3D printed PLA/CS scaffolds was examined. Two Gram-positive and two Gram-negative standard pathogenic bacteria (*Staphylococcus aureus* ATCC 29213, *Enterococcus faecalis* ATCC 29212, *Escherichia coli* ATCC 25922, *Pseudomonas aeruginosa* ATCC 27853) were used to study with the agar disk diffusion method. Fresh subcultures on 5 % sheep blood agar of bacteria were used to adjust 0.5 McFarland turbidity standard solutions (1.5 × 108 CFU/mL) in tubes containing sterile saline. Processed bacterial solutions were inoculated on Muller Hinton Agar with a sterile swab. Disks (5 mm in diameter) were cut from different concentrations ST loaded 3D printed scaffolds and exposed to UV light (254 nm) for 1 h for sterilization. Sterilized disks were placed on the surface of bacteria-inoculated Mueller-Hinton agar (bioMérieux) plates. Sterile disks containing levofloxacin (5 μg) were used as a positive control for all bacteria. Plates were incubated at 37 °C for 18 h, and growth inhibition zones around disks were measured and evaluated according to the European Committee on Antimicrobial Susceptibility Testing (EUCAST) criteria [22].

### 2.7. Cell viability assay

Human fibroblast cells (CCD-1072Sk) were purchased from American Type Culture Collection (ATCC) and maintained in Dulbecco's modified Eagle medium containing 10 % fetal bovine serum and 100UI/ml penicillin/streptomycin at 37 °C in a 5 % $CO_2$ incubator. Cell viability was determined using Thiazolyl Blue tetrazolium bromide (MTT) reagent (Alfa Aesar, Thermo Scientific). Before treatment of the cells, scaffolds (PLA only, PLA/CS, PLA/CS/1 %, 2 %, 3 %, 5 %, 10 % and 15 % wt ST) were cut into equal pieces (1 cm × 1 cm) for each well and sterilized under UV for at least 1 h. Cells were seeded into 24 well plates at a density of 5 × 104 cells/well and were incubated with scaffolds for 24, 48, and 72 h. At the end of the incubation, scaffolds were removed and MTT reagent was added to each well with a final concentration of 0.1 mg/ml, and cells were further incubated for 2 h at 37 °C in a 5 % CO2 incubator till formazan crystals were observed under microscopy. All the media inside the wells were discarded and DMSO was added to each well. Absorbance values were read at 570 nm by Thermo Multiskan GO microplate spectrophotometer (Fisher Scientific). Cell viability was calculated according to Eq. (5):

$$\text{Cell viability}\% = (\text{Mean absorbance of the treatment})/(\text{Mean absorbance of the control}) \times 100 \quad (5)$$

### 2.8. Wound healing assay

CCD-1072Sk cells were plated on 6 well plates at a density of $2 \times 10^5$ cells/well and incubated with scaffolds (PLA only, PLA/CS, PLA/CS/1 %, 2 %, and 3 % wt ST) for 24, 48, and 72 h. A scratch with constant width was done in the monolayer of cells using a 200 μl pipette tip. Cells were washed twice with PBS to remove any suspended cells and further cultured in a media. Wound closure was monitored at different time points (24, 48, and 72 h) with brightfield microscopy and analyzed by using the ImageJ MRI wound healing tool.

### 2.9. Apoptosis assay

Apoptotic and necrotic cells were determined by using Annexin V-Propidium Iodide staining. CCD-1072Sk cells were incubated with scaffolds (PLA only, PLA/CS, PLA/CS/1 %, 2 %, and 3 % wt ST) for 72 h and washed with cold PBS (1×) twice and then $1 \times 10^6$ cells were suspended in 1× Binding Buffer. The rest of the assay was performed by the manufacturer's instructions (Annexin V:FITC Assay Kit, Bio-Rad). Stained cells were acquired by using BD Accuri C6 Flow Cytometer and data were analyzed by using Kaluza Analysis Software (Beckman Coulter).

### 2.10. Statistical analysis

Statistical analysis and pore size measurements of tissue scaffolds were performed using the SPSS 17.0 analysis program. One-way analysis of variance was used to test whether there was a statistically significant difference between the means of independent groups. The significance level was determined as $p < 0.05$ and data were labeled with (*) for $p < 0.05$ and (**) for $p < 0.005$.

## 3. Result and discussion

### 3.1. Morphological and rheological analysis of 3D printed scaffolds

The basic fabrication process of 3D printed PLA/CS based composite scaffolds for wound dressing application is illustrated in Fig. 1.

In order to develop printable PLA/CS based ST loaded ink solutions, the rheological behaviors of PLA and PLA/CS based 3D printing solutions were evaluated and optimized to determine the optimal ink formulation for 3D printing. The three different concentrations of ST (1 %, 2 %, and 3 % wt) loaded into PLA/CS solution were selected as optimal ink formulations for feasibility during the 3D printing process. The optimized rheological properties including viscosity, surface tension, and density of 3D printed scaffolds are given in Table 1. Besides, the macrographs of 3D printed pure PLA, PLA/CS, and different concentrations of ST loaded PLA/CS scaffolds with optimized solution parameters were also given in Table 1.

Among the rheological properties, especially the viscosity of the 3D printing solution has a direct impact on achieving high-resolution printing through precise three-dimensional extrusion [23].

**Table 1**
The macrographs of the scaffolds and the rheological properties of the solutions.

| 3D scaffold images | 3D scaffold composition (% wt) | Viscosity (mPa.s) | Density (kg/m$^3$) | Surface Tension (mN/m) | Pore size (μm) |
|---|---|---|---|---|---|
|  | PLA | 2273 ± 13.05 | 1416 ± 30 | 28.23 ± 0.15 | 519.62 ± 10.51 |
|  | PLA/CS | 4995 ± 7.81 | 1262 ± 20 | 27.47 ± 0.99 | 512.68 ± 14.18 |
| 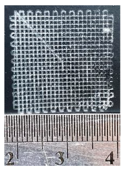 | PLA/CS/1 % ST | 5331 ± 7.09 | 1265 ± 20 | 26.63 ± 1.02 | 581.99 ± 29.34 |
| 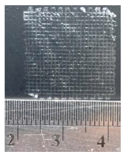 | PLA/CS/2 % ST | 5004 ± 4.50 | 1273 ± 30 | 30.77 ± 1.84 | 525.73 ± 39.32 |
| 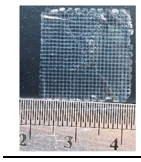 | PLA/CS/3 % ST | 975 ± 5.00 | 1269 ± 30 | 29.53 ± 0.51 | 476.22 ± 43.71 |

PLA is an excellent polymer for 3D printing due to its good rheological properties which do not degrade when extruded [24]. However, it has a hydrophobic surface structure and has no functional groups that promote bioactivity [25]. In this study, PLA was reinforced with CS, a natural polymer, to enhance the bioactivity of 3D printed scaffolds. The pure PLA 3D printing solution exhibited good printability as can be seen in the macrograph of the pure PLA 3D printed scaffold in Table 1. The 3D printed scaffolds were fabricated as 7 layers with uniform opened pores and the printed strips did not show any tendency to spread. These results can be seen clearly in SEM images with a pore diameter of 519,62 μm (Fig. 2a). In addition, no clogging was observed at the needle tip during extrusion under constant mechanical pressure. These results are directly related to the well-adjusted rheological properties of the 15 % (*w/v*) PLA solution. In order to increase the biological functionality of PLA, CS was added to the optimized 15 % (w/v) PLA solution, and rheological analysis of the mixed solutions was performed for the fabrication of PLA/CS composite 3D printed scaffolds. CS is known to improve cell adhesion, proliferation, and differentiation, but shows very poor mechanical properties [26]. In the literature, there are studies in which PLA/CS based biomaterials with high mechanical strength and bioactivity are produced and applied by combining PLA mechanical strength with CS bioactivity, especially in tissue engineering applications [24,26]. Also, when CS is applied to wounds, it helps with blood clotting [27]. From this point of view, a 3D printed PLA/CS based composite scaffold was considered to be a suitable carrier platform in this study, which is aimed at wound healing patch fabrication.

The macrograph of the PLA/CS based 3D printed scaffold which is prepared by mixing the 15 % PLA (*w/v*) and 2 % (w/v) CS solution can be seen in Table 1. The optimized rheological properties of PLA/CS solution can be also seen in Table 1.

In the PLA/CS SEM image (Fig. 2b), it can be clearly seen that the square pore structures with the overlapped layer strips are easily distinguishable from each other which is similar to the SEM image of PLA (Fig. 2a). The macrograph and SEM images revealed that this PLA/CS solution feasibility is suitable for 3D printing, although the PLA/CS solution viscosity value (4495 mPA.s) is approximately 2 times higher than the PLA solution. This result is consistent with the literature. In the study of Elviri et al., 3D printing studies were carried out with different concentrations of CS solution. Raffinose was added to the CS solution as a viscosity modifier [28]. The study revealed that the viscosity of the CS solution plays a fundamental role in the printability and final structural quality of the 3D printed scaffolds. The group prepared the different concentrations of CS solution varying between 5 and 7 % (*w/v*) and the obtained suitable viscosity values increased from 5000 to 45,000 cP. In the study, 3D printability was properly achieved at all these viscosity levels. Ilhan et al. carried out 3D printing studies with PLA/CS solutions with 15 % (wt) PLA solution and different concentrations of CS, 1 %, 3 %, and 5 % (wt) [19]. They revealed that low concentrations of CS (1 % wt) reduced viscosity and this led to the spread of strips, while high concentrations of CS (5 % wt) increased viscosity and caused clogging of the needle when mixed with 15 % wt PLA. Therefore, in the study, the solution containing 3 % (wt) CS with 15 % (wt) PLA was selected as a suitable solution for 3D printing.

Thus, in this study, the optimized PLA/CS with 15 % PLA (wt) and 2 % CS (wt) solution was determined as the ST carrier scaffold. The different concentrations of ST as 1 %, 2 %, and 3 % (wt) were added to the optimized PLA/CS solution. When the macrographs given in Table 1 and SEM images (Fig. 2c, d, e) were compared, it was observed that as the ST ratio increased, the scaffold strips tended to spread and layer clarity decreased. This result was also associated with decreasing viscosity values as ST increased. As can be seen from the SEM images, the 3 % (wt) ST loaded 3D printed scaffold exhibited strip spreading due to the

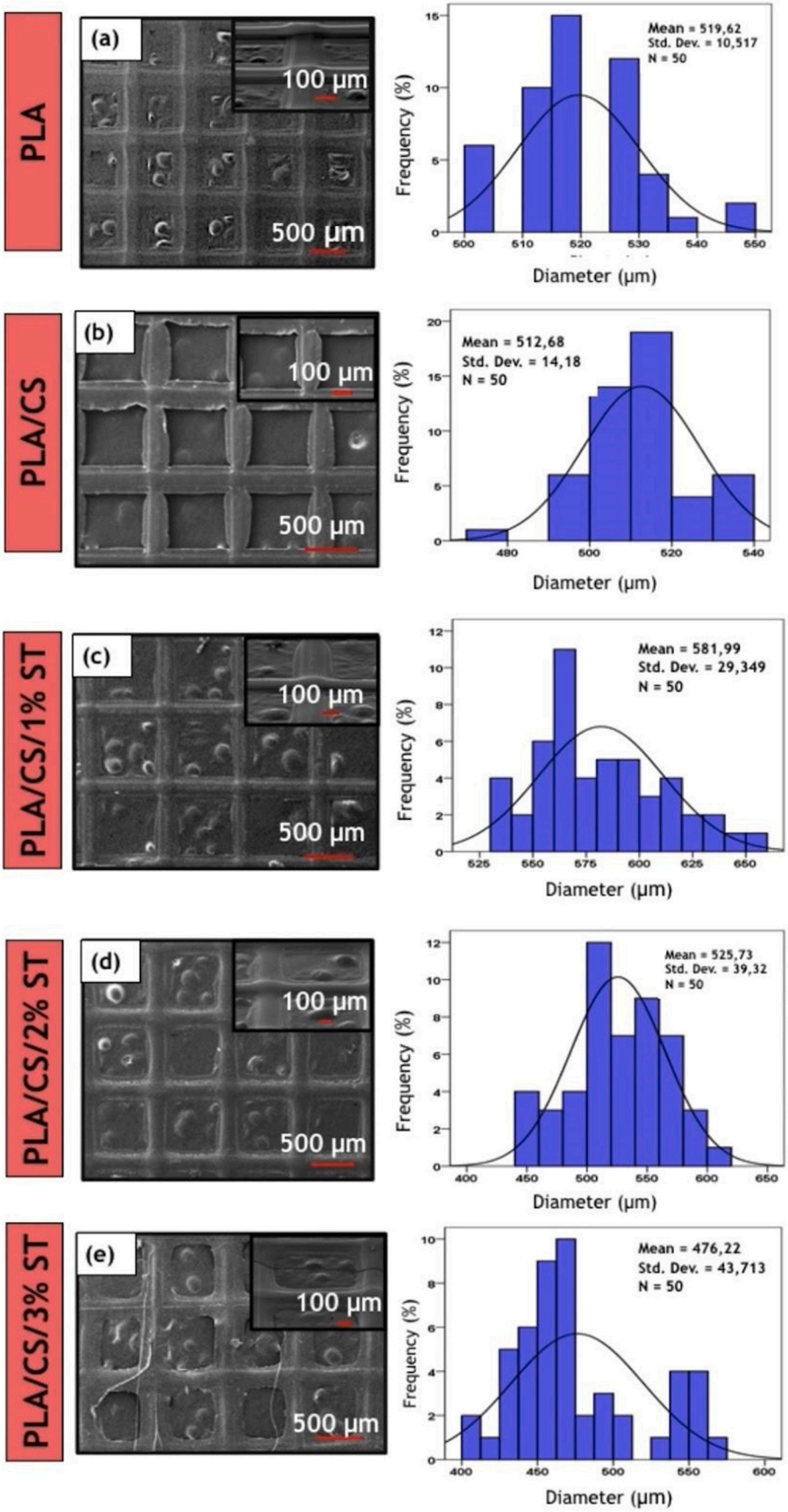


**Fig. 2.** SEM images and pore size analysis of PLA (a), PLA/CS (b), PLA/CS/1 % ST (c), PLA/CS/2 % ST (d), PLA/CS/3 % ST (e), scaffolds.

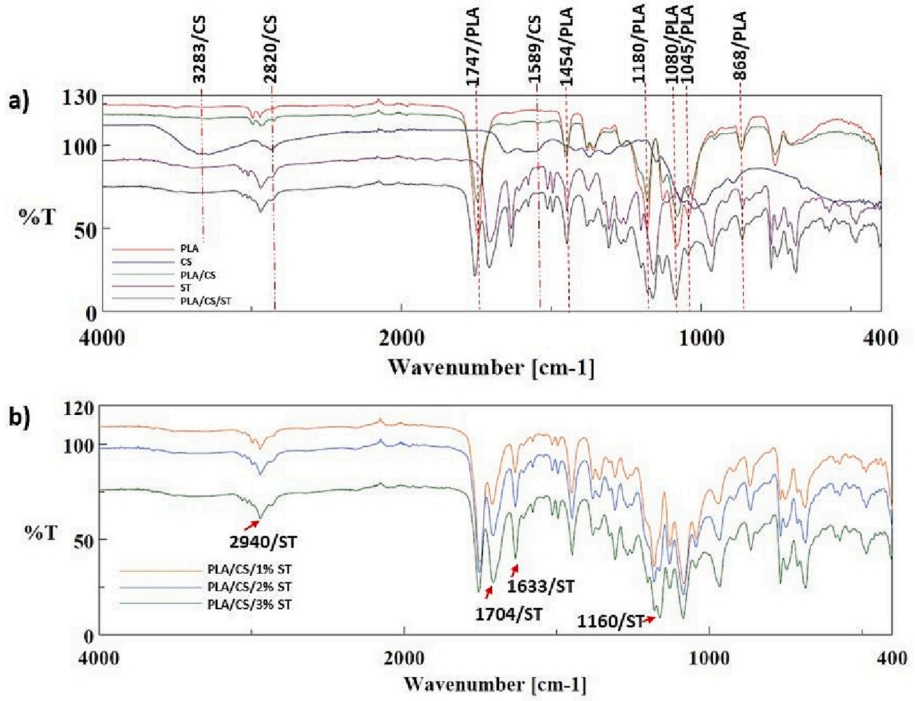


**Fig. 3.** FT-IR spectrum of pure PLA, CS, ST, 3D printed PLA/CS, 3D printed PLA/CS/ST (a), and FT-IR spectrum of different amounts of ST loaded 3D printed PLA/CS/ST (b).

very low viscosity compared to other composite solutions. This spreading resulted in the ovalization of the square pore structure and thus resulted in a smaller diameter size compared to other scaffolds.

For proper 3D printing, the value of the surface tension is just as important as the value of the viscosity. The surface tension of the solution used determines the shape of the solution exiting the needle tip and its adhesion to the print surface. The surface tension value should generally be between 28 and 350 mN $m^{-1}$, which is suitable for additive manufacturing [29]. As can be seen in Table 1, the surface tension values were suitable for 3D printing for all compositions.

### 3.2. Fourier transform infrared spectroscopy (FT-IR)

FT-IR spectra of pure PLA, CS, ST, 3D printed PLA/CS, 3D printed PLA/CS/ST, and FT-IR spectra of different concentrations of ST loaded 3D printed PLA/CS/ST were presented in Fig. 3 (a, b) respectively. Pure PLA (C═O vibration peak at 1747 $cm^{-1}$, $CH_3$ asymmetrical scissoring at 1454 $cm^{-1}$, C—O asymmetrical stretching and $CH_3$ twisting at 1180 $cm^{-1}$, C-O-C stretching at 1080 $cm^{-1}$, C-$CH_3$ stretching at 1045 $cm^{-1}$ and C-COO stretching at 868 $cm^{-1}$) [18] and pure CS (N—H stretching at 3283 $cm^{-1}$, C—H vibration at 2820 $cm^{-1}$ and primary amide C═O stretching at 1589 $cm^{-1}$) [30] characteristic peaks were obtained (Fig. 3**a**). It was also clearly seen that the characteristic peaks of PLA and CS were located in the 3D printed PLA/CS scaffold spectrum that C═O

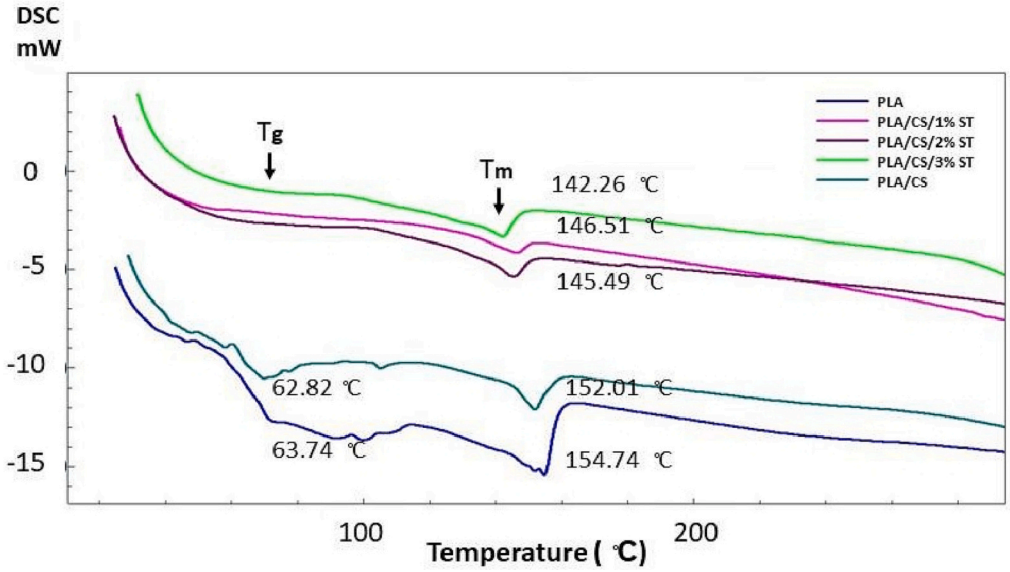


**Fig. 4.** DSC thermogram of the PLA, PLA/CS and different amounts of ST loaded 3D printed PLA/CS/ST.

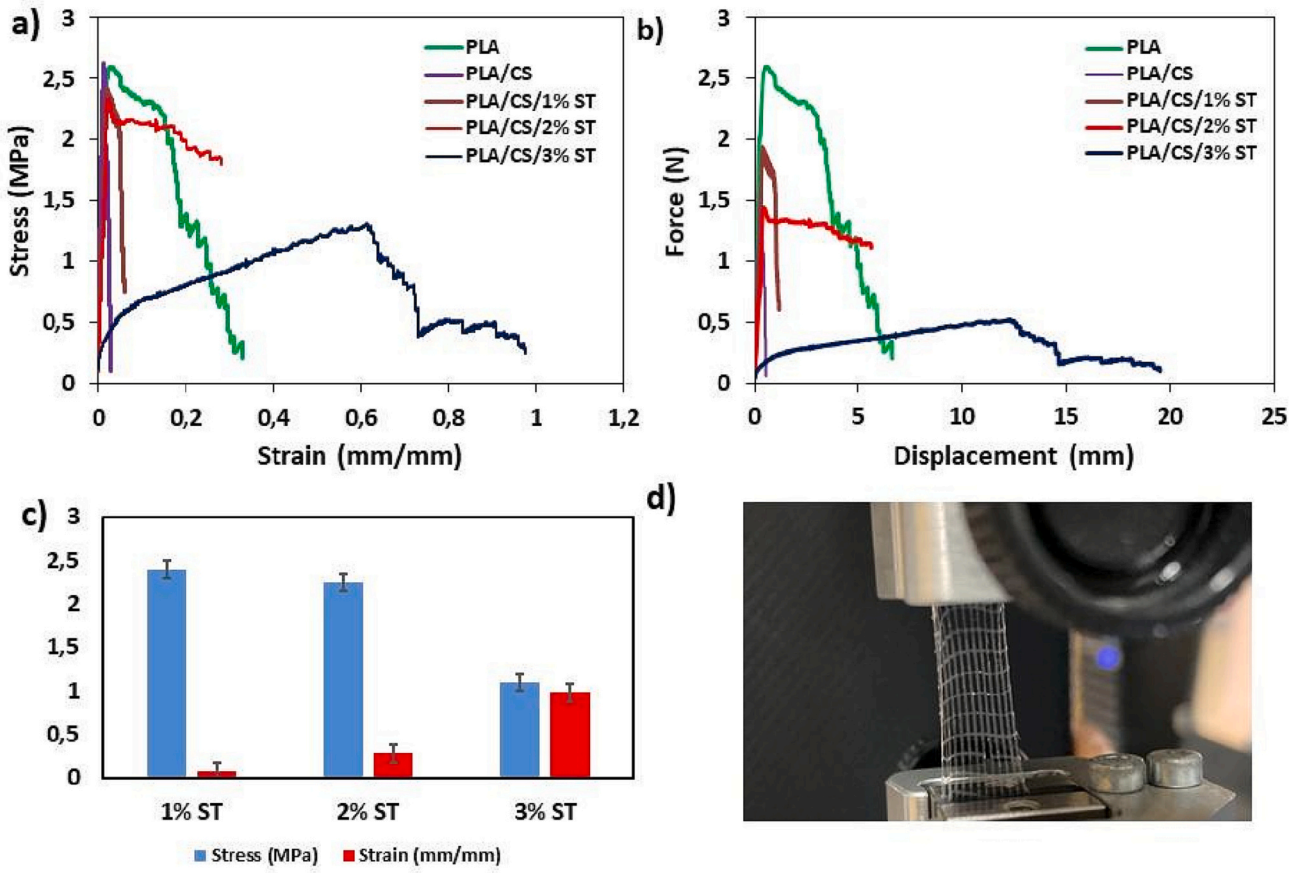


**Fig. 5.** Mechanical test results of all scaffold for stress/strain (a), force vs. displacement (b), comparing of stress vs strain values for different amount of ST loaded scaffolds ©, digital image of tensile test of PLA/CS/ 3 % ST scaffold.

at 1747 $cm^{-1}$ and C—H at 2820 $cm^{-1}$, respectively (Fig. 3a). This coexistence of the characteristic peaks of PLA and CS at the 3D printed PLA/CS spectrum revealed that PLA/CS scaffolds have been produced successfully. For pure ST, related peaks were found at 2940 $cm^{-1}$, 1704 $cm^{-1}$, 1633 $cm^{-1}$, and 1160 $cm^{-1}$ which were marked in Fig. 3b [31]. Demir et al. stated that the peak at around 1640 $cm^{-1}$ corresponding to the double bond stretching vibration corresponds to C═C styrene which is the main component of styrax [31]. In Fig. 3a, the characteristic bonds of PLA, CS, and ST were clearly observed in the PLA/CS/ST spectrum. This result revealed that ST was successfully loaded into 3D printed PLA/CS scaffolds.

Additionally, Fig. 3b demonstrates the changes in chemical bonding that can occur when loading different concentrations of Styrax into 3D printed PLA/CS scaffolds. In the spectra of the PLA/CS scaffolds loaded with ST (Fig. 3b), it can be clearly seen that the spectral intensity of the peaks has increased with the increase in the concentrations of ST.

### 3.3. Differential scanning calorimetry (DSC)

The thermal properties of different concentrations of ST loaded PLA/CS based 3D printed scaffolds were investigated by DSC thermograms to observe the ST effect on the glass transition temperature ($T_g$) and melting temperature ($T_m$). The DSC curves with $T_g$ and $T_m$ values of PLA, PLA/CS, and different concentrations of ST loaded PLA/CS 3D printed scaffolds are shown in Fig. 4.

The results of the DSC analysis demonstrated that $T_g$ and $T_m$ values of 3D printed PLA scaffolds were compatible with the literature [32]. As can be seen in Fig. 4, the 3D printed PLA scaffolds had Tg and Tm values of 63.74 °C and 154.74 °C, and the PLA/CS scaffolds had $T_g$ and $T_m$ values of 62.82 °C and 152.01 °C, respectively. The fact that PLA/CS scaffolds have a lower melting point than PLA scaffolds can be explained by the effect of the amorphous structure of CS on the melting point of PLA. Similar results were found in the study by Nguyen et al. [33]. On the other hand, the $T_g$ and $T_m$ values of PLA/CS scaffolds decreased with an increasing amount of ST. This result can be explained by the plasticizing effect of ST on PLA. Studies using different types of oil in polymer-based biomaterials have shown similar results [32,34].

### 3.4. Mechanical properties of the 3D printed scaffolds

The changes in the mechanical behavior of PLA/CS based 3D printed scaffolds caused by the addition of different amounts of ST are shown in Fig. 5 (a-d). A sharp decrease was observed in the strain value of PLA/CS scaffolds (0.02 ± 0.24 mm/mm) by CS addition to PLA scaffold (0.32 ± 0.06 mm/mm), while there was no significant change in the stress values. It can be clearly seen in Fig. 5b that the PLA scaffold achieved a maximum force of 2.59 (N) with an elongation at a break of 6.6 mm, the PLA/CS scaffold achieved a maximum force of 1.06 (N) with an elongation at break of 0.50 mm. Nguyen et al. have observed the same reduction in strain value in the production of PLA/CS core/shell nanofiber mats in comparison to PLA nanofiber mats [33]. In addition, a direct proportional increase was observed in the strain values of the scaffolds with the addition of 1 % and 2 % (wt) ST. On the other hand, the addition of ST resulted in a slight decrease in stress values compared to PLA and PLA/CS 3D printed scaffolds (Fig. 5 a-c). When 3 % (wt) ST was added to PLA/CS scaffolds, significant changes occurred in both strain and stress values (Fig. 5 a-d). Compared to all other scaffolds, the stress value decreased to 1.09 ± 0.12 MPa, while the strain value increased to 0.98 ± 0.06 mm/mm. Nejati-Koshki et al. have observed the same improvement in elongation with the addition of emu oil extract

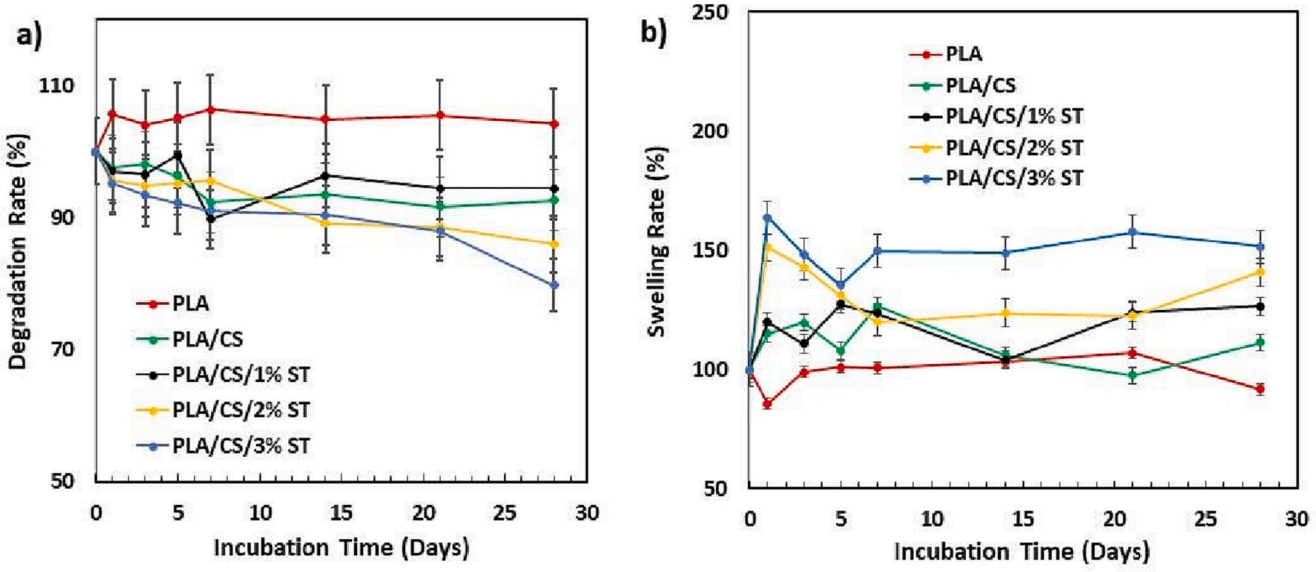


**Fig. 6.** Degradation(a) and Swelling (b) of PLA, PLA/CS and different amounts of ST loaded 3D printed PLA/CS/ST scaffolds in PBS 7.4 at 37 °C.

to PCL/collagen nanofibers [35]. Besides, the sharp decrease in viscosity of the 3 % (wt) ST loaded 3D printing solution may also be the cause of the reduction in stress value compared to the others (Table 1). On the other hand, the mean pore size of the 3D printed scaffold loaded with 3 % (wt) ST was 476.22 ± 43.71 nm, which was the lowest value of the pore diameter compared to the others. Ilhan et al. loaded Satureja cuneifolia (SC) into sodium alginate (SA)/polyethylene glycol (PEG)-based 3D printed scaffolds at different ratios. The same study found that the tensile strength of the lowest pore-size scaffolds decreased with SC loading [19].

In the stress/strain curve, it can be clearly seen that the tensile stress of the 3D printed scaffolds increases with increasing amounts of ST (in weight %). It has been reported in the literature that human skin has a tensile strength in the range of 1–32 MPa and a tensile strain in the range of 17–207 % [36]. On the basis of these values, it can be said that 2 % and 3 % (wt) ST loaded PLA/CS scaffolds have mechanical properties in

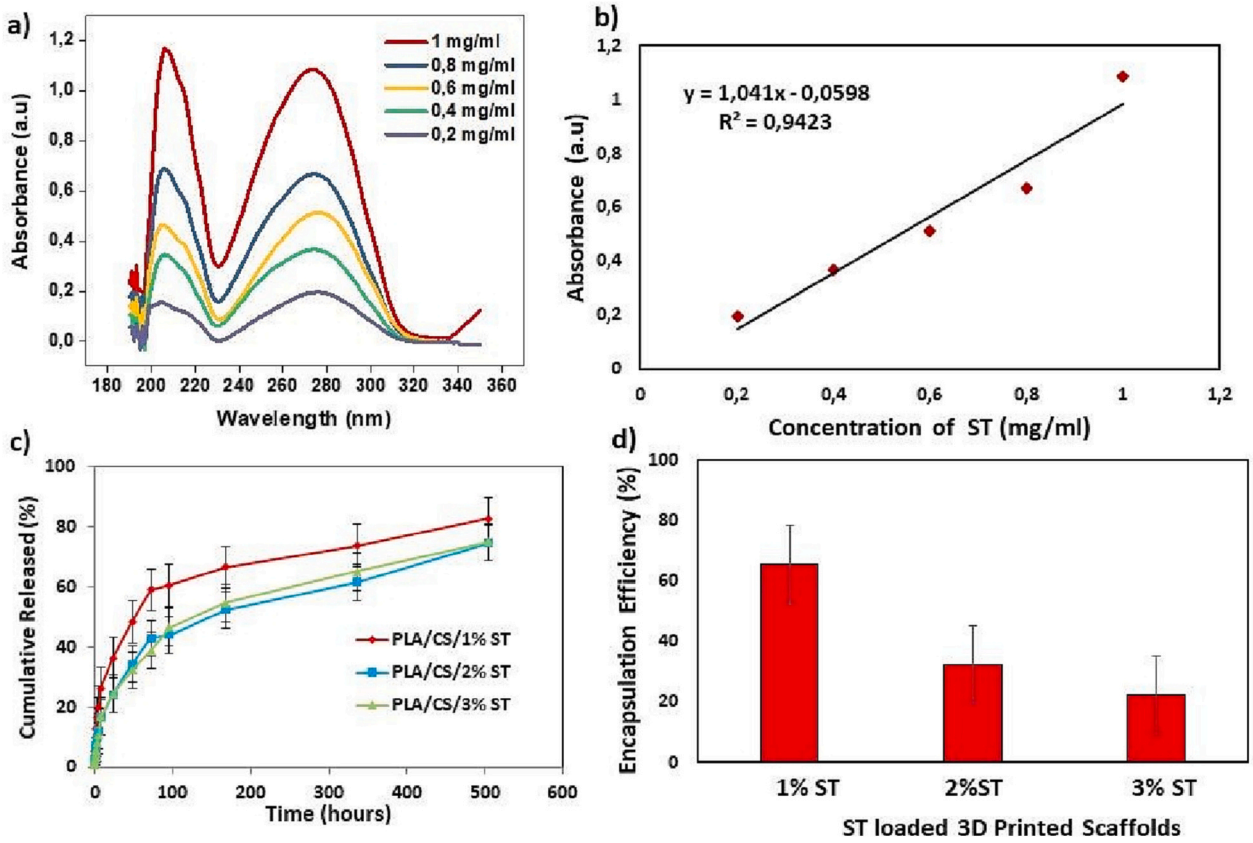


**Fig. 7.** Absorption spectra of ST at different concentrations (a), Calibration curve of ST (b) and (c) Cumulative ST release profiles from different amounts ST loaded PLA/CS/ST 3D scaffolds, and Encapsulation efficiency of ST loaded 3D PLA/CS/ST scaffolds (d).

the range which are suitable for tissue engineering and wound dressing applications. Given that the resistance of the dressing material to different human tissue pressures is related to its durability [37], it can be said that the scaffolds loaded with increasing amounts of ST (% wt) are durable wound dressings.

### 3.5. Swelling and degradation behaviors of scaffolds

In tissue engineering applications, biodegradable scaffolds can be seeded with cells and growth factors to enable tissue regeneration, while in smart drug delivery systems, the loaded drug is released from biodegradable scaffolds to deliver the drug to the target tissue [38,39]. The biodegradability of the 3D printed scaffolds was investigated in Fig. 6a, which shows the weight loss of PLA, PLA/CS, and ST loaded scaffolds in PBS (pH 7.4) at predetermined time points.

As seen in Fig. 6a, the weight loss of the 3D printed PLA scaffolds was very low. This result confirms that PLA, in relation to its hydrophobicity and biological inertness, has the disadvantages of low cell adhesion and low degradation rate [40]. This low biodegradation rate of PLA results in low ST release from PLA scaffolds and prevents water and living cell populations from penetrating PLA scaffolds [41]. For an ideal biomaterial to exhibit good biocompatibility, it must have a good degradation rate. To this end, CS biopolymer was added to the polymer structure to increase the biocompatibility of the 3D printed scaffold. CS is widely preferred in tissue engineering studies due to its high biocompatibility and biodegradability. As expected, the addition of CS to the 3D printed scaffolds resulted in a significant increase in the degradation rate of PLA/CS (Fig. 6a). Also, the increase in the degree of swelling can be attributed to the hydrophilic nature of CS, which has the effect of increasing the water absorption capacity [42]. In addition, it was observed that the degradation rate of PLA/CS 3D printed scaffolds increased when increasing concentrations of ST was added. As shown in Fig. 6a, the 3 wt% ST loaded scaffolds showed approximately 22 % degradation. While the degradation rate was observed as 15 % of the scaffold loaded with 2 % wt ST, the degradation rate of the 1 % wt ST loaded scaffold was determined as 7 %. The degradation results are also directly related to the swelling properties of the scaffolds. The swelling profiles of the scaffolds were given in Fig. 6b. Depending on the degradation rates, the highest swelling rate was observed in the scaffold loaded with 3 wt% ST, which reached up to 151 %, followed by the scaffold loaded with 2 wt% ST with 140 %. These results are consistent with the literature. In their study, Demir et al. loaded ST into PCL nanofibers at different rates and observed that the water absorption capacity of the samples increased as the ST ratio increased. They attributed this result to the improvement in the hydrophilic properties of the samples with the addition of ST [17]. The study found that pure PCL membranes with a hydrophobic structure became slightly hydrophilic with the addition of ST. The good degradation and swelling properties of ST loaded PLA/CS scaffolds indicate that cells can attach, spread and proliferate on these scaffolds at any time.

### 3.6. In vitro ST release profiles and kinetic assays

A standard calibration curve was plotted using the absorbance values at 274 nm in the UV spectra taken from the concentration range of ST between 2 and 10 mg/ml to calculate the release of ST, loaded into the 3D printed scaffolds, from the polymer matrix into the PBS media (Fig. 7a and b). The ST calibration curve ($y = 1041\times$-0,0598, $R2 = 0.9423$) was used to calculate the concentration of ST in the PBS media (pH 7.4). The time-dependent cumulative curves of ST release from 3D printed scaffolds at different concentrations are shown in Fig. 7c.

As can be observed in Fig. 7c, all ST concentrations (1 %, 2 %, and 3 % wt) showed sustained release profiles in the first 24 h, which were 36.2, 24.10, and 24.43 % of the total amount of ST, respectively. At the end of 21 days, the release profiles reached 82.69 %, 74.61 %, and 74.89 % of the total ST amount, for 1 %, 2 %, and 3 % wt ST loaded scaffolds, respectively. These results indicated that sustained release of ST could last over 1 month. The sustained controlled release of ST from 3D printed scaffolds over time has demonstrated that these biomaterials can be used as a direct, effective wound healing material when applied locally to damaged tissue.

The release data were also fitted to the various kinetic models to evaluate the kinetics and mechanism of ST release from 3D printed PLA/CS based scaffolds for all formulations. Zero order, first order, Higuchi's, Hixson-Crowell, and Korsmeyer–Peppas models were evaluated for all formulations, respectively. The kinetic rate constant (k), the correlation coefficient (R2), and for the Korsmeyer-Peppas model the release exponent (n) were given in Table S1.

It was found that the in vitro drug release of ST with different amounts was best fitted by Higuchi's equation, as the plots showed the highest linearity ($R2 = 0.9078$), ($R2 = 0.9607$) and ($R2 = 0.9661$) for 1 %, 2 %, and 3 % wt ST loaded 3D printed scaffolds, respectively. The high linearity of the fit shows that the drug diffuses at a comparatively slower rate as the diffusion distance increases, which can be explained by square root kinetics (or Higuchi kinetics) [43].

The encapsulation efficiency (EE) of different concentrations of ST loaded PLA/CS based 3D printed scaffolds was calculated and given in Fig. 7d. As can be seen from the bar graphs, the highest EE% belongs to the 1 % concentration with 65.93 %.

Wounds occur as a result of deterioration in the anatomical and functional integrity of living tissue. Wound healing is defined as the formation of new tissue as a result of regular and sequential cellular and biochemical events following this deterioration. The healing of wounds is an extremely complex process [44]. In a nutshell, it is made up of four phases and hemostasis can be achieved through the correct progression of these inflammatory, proliferative, and remodeling phases (Fig. 8).

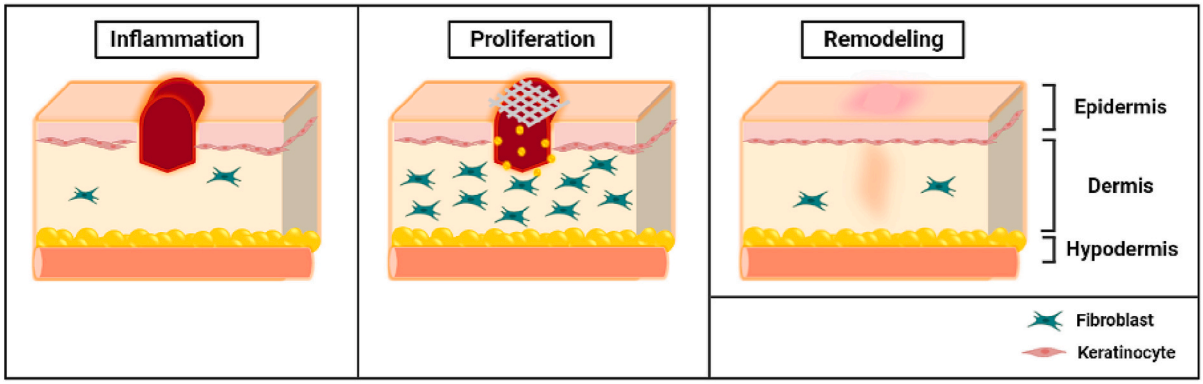


**Fig. 8.** Schematic illustration of wound healing phases consisting of inflammation, proliferation, and remodeling phases along with sustained ST release from 3D printed PLA/CS based 3D scaffold and its effect on wound healing process.

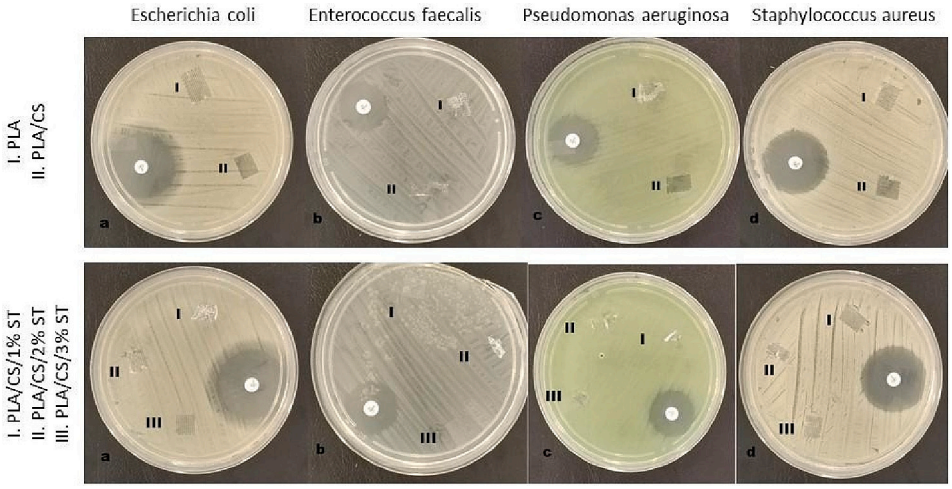


**Fig. 9.** The inhibition zone of PLA and PLA/CS 3D printed scaffolds and levofloxacin (5 μg) against 4 standard pathogenic bacteria (*Escherichia coli* ATCC 25922, *Enterococcus faecalis* ATCC 29212, *Pseudomonas aeruginosa* ATCC 27853, *Staphylococcus aureus* ATCC 29213 from a to d, respectively) after 18 h incubation at 37 °C. No zone was detected in 3D printed scaffolds (up). The inhibition zone of different concentrations of ST loaded 3D printed scaffolds and levofloxacin (5 μg) against 4 standard pathogenic bacteria after 18 h incubation at 37 °C. No inhibition zone was detected at different doses of loaded 3D printed scaffolds on each bacteria (bottom).

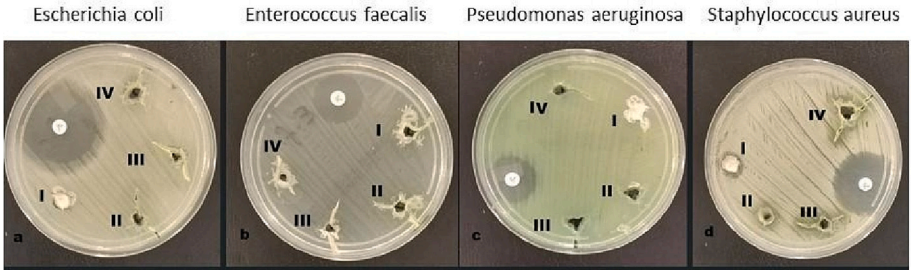


**Fig. 10.** The inhibition zones of incubation media of different amount of ST loaded 3D printed scaffolds and levofloxacin (5 μg) against 4 standard pathogenic bacteria (*E. coli* ATCC 25922, *E. faecalis* ATCC 29212, *P. aeruginosa* ATCC 27853, *S. aureus* ATCC 29213, respectively after 18 h incubation at 37 °C as I- ST itself (12 mm), II- incubation media of loaded PLA/CS/1 % ST (11 mm), III- incubation media of loaded PLA/CS/2 % ST (10 mm), IV- incubation media of loaded PLA/CS/3 % ST (10 mm).

**Table 2**
The inhibition zone values of free ST, the incubation media of ST loaded 3D scaffolds and levofloxacin (5 μg) against four standard pathogenic bacteria: *E. coli* ATCC 25922, *E. faecalis* ATCC 29212, *P. aeruginosa* ATCC 27853, *S. aureus* ATCC 29213.

| | *Escherichia coli* | *Enterococcus faecalis* | *Pseudomonas aeruginosa* | *Staphylococcus aureus* |
|---|---|---|---|---|
| (Levofloxacin)[a] (up) (Fig. 9) | 31 | 22 | 29 | 22 |
| (Levofloxacin)[a] (btm) (Fig. 9) | 33 | 22 | 29 | 22 |
| (Levofloxacin)[a] (Fig. 10) | 33 | 22 | 29 | 22 |
| ST (free) (Fig. 10) | 0 | 0 | 0 | 12 |
| PLA/CS/%1 ST (media) (Fig. 10) | 0 | 0 | 0 | 11 |
| PLA/CS/%2 ST (media) (Fig. 10) | 0 | 0 | 0 | 10 |
| PLA/CS/%3 ST (media) (Fig. 10) | 0 | 0 | 0 | 10 |

[a] All inhibition zones detected with Levofloxacin were in expected normal intervals according to EUCAST Quality Control Standards. All inhibition zone diameters are in mm.

The basic principle of wound healing is to provide adequate tissue perfusion and oxygenation, and an appropriate nutritional and hydration environment to maintain the anatomical and functional integrity of the affected area [45].

### 3.7. Antibacterial assay

The results of the antibacterial activity of PLA, PLA/CS and different amounts of ST loaded PLA/CS/ST 3D printed scaffolds with agar disk diffusion tests were given in Fig. 9. However, no antibacterial activity was observed against four standard bacteria with different concentrations of ST loaded PLA/CS 3D printed scaffolds, while the antibacterial activity of diluted 200 μg ST (free) was observed only against *Staphylococcus aureus* ATCC 29213. Okmen et al. also found the antibacterial activity of ST extracts in three different solvents (acetone, ethanol, and methanol) against *Staphylococcus aureus* showing a 12 mm zone of inhibition as we observed [46]. Extracts of ST showed antibacterial activity against *Staphylococcus aureus* and some other bacteria while they did not show against *Escherichia coli* [47]. In the antibacterial assay, the most common bacterial species were chosen which were isolated from wounds and abscesses and these bacterias are *E. coli* [22], *E. faecalis* [46], *P. aeruginosa* [47], and *S. aureus* [48]. Among them, especially *S. aureus* is a highly colonized bacteria in the wound environment [48,49]. According to the obtained results, it can be thought that ST loaded 3D printed scaffolds release ST slower than the growth rate of the selected bacteria. This may be one reason why *S. aureus* is resistant to 3D printed ST loaded scaffolds while being sensitive to ST itself. However, considering that these scaffolds can release ST in a biological environment in a controlled manner, it can be thought that the rates of ST released in biological environment conditions will increase proportionally with the release analysis. In addition, it was also observed zone diameters in expected normal intervals against levofloxacin according to EUCAST criteria [50].

The results of the antibacterial activity of PLA, PLA/CS, and different concentrations of ST loaded PLA/CS/ST 3D printed scaffolds with agar disc diffusion tests are shown in Fig. 9.

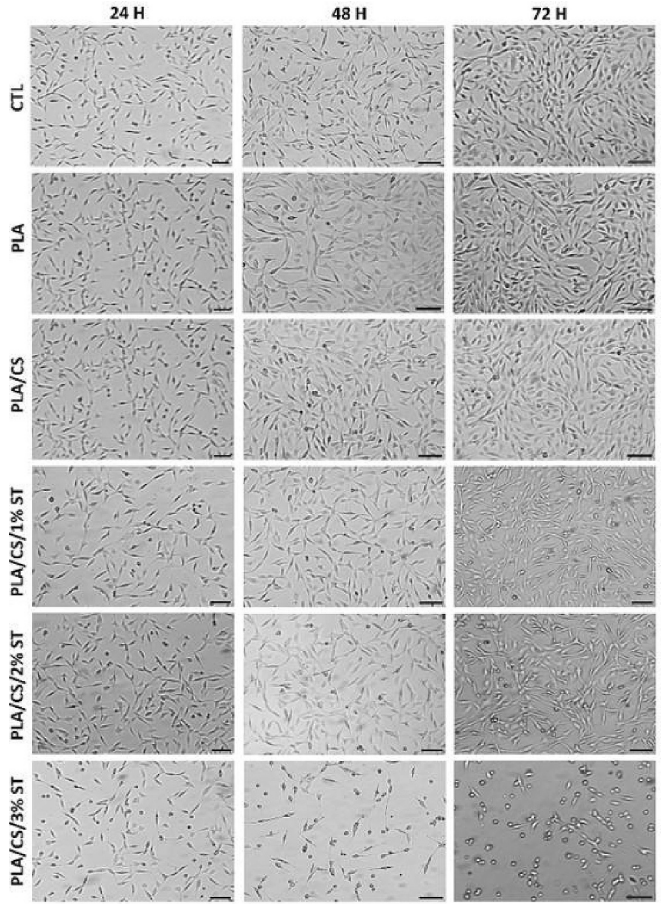


**Fig. 11.** Brightfield images for high concentrations of ST induces cell death on human fibroblast cells for 24, 48 and 72 h. Scale bar: 50 μm.

Since no inhibition zones could be obtained from the antibacterial tests of the directly ST loaded 3D printed scaffolds, the different amounts ST loaded 3D printed scaffolds were incubated in PBS for 24 h to mimic the biological environment and the antibacterial activities of the incubation media were tested by using agar disc diffusion method. The agar disc diffusion test results of incubation media of ST loaded PLA/CS/ST 3D printed scaffolds in PBS for 24 h are shown in Fig. 10.

As can be seen in Fig. 10, the inhibition zones were observed against only *S. aureus* bacteria both free ST and all different concentrations of ST loaded 3D printed scaffold incubation media. The inhibition zone diameters (mm) were given in Table 2.

The obtained results showed that despite no inhibition zones could be obtained from the antibacterial tests of the directly ST loaded 3D printed scaffolds against *S. aureus* strains, antibacterial activities against *S. aureus* strains were seen with their incubation media in PBS for 24 h. It can be said that the hydrophobic structure of PLA prevents sufficient ST release from ST loaded PLA/CS based 3D printed scaffolds in agar medium for effective antibacterial effect, and therefore inhibition zones against *S. aureus* strains are not observed. In addition, as previously mentioned the biological environment triggers the release mechanism as it initiates the biodegradation of the active agent loaded biopolymers. In the antibacterial tests carried out with the media of the samples loaded with ST at three different concentrations and incubated in PBS for 24 h, the size of inhibition zones were observed at approximately the same rate as with the free ST. When the results are compared with the release analyses, they are in agreement, considering that approximately 25 % of the ST was released from ST loaded samples at each concentration at the end of the first 24 h.

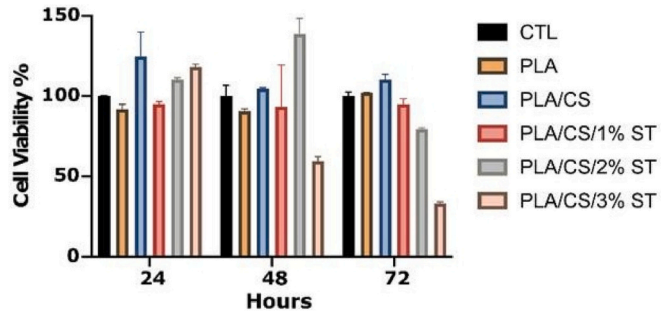


**Fig. 12.** Cell viability of CCD-1072Sk cells incubated with different scaffolds containing various concentrations of ST for 24, 48 and 72 h. Columns show mean values of three independent experiments (±SD). SD, standart deviation.

*S. aureus* can be colonized in the human skin and in the nasal vestibules [51]. After colonization, it could cause many types of infections such as infected diabetic foot ulcers [52], chronic wound infections [53], infected pressure ulcers [54]. Other important infections caused by *S. aureus* have been diagnosed in patients hospitalized in intensive care units. The bacteria was shown to cause pneumonia in mechanically ventilated patients, and their mortality rate was high compared with other microorganisms and uninfected patients [55].

This wide range of infections and the ability of *S. aureus* to develop resistance to antimicrobial drugs has led scientists to look for new ways to combat it [56]. It is important to neutralize the microbe at the site of colonization before it causes infection or septicemia. The antibacterial activity of ST against *S. aureus* that we have observed in our tests could provide an idea for new research into the prevention of infections and sepsis that could be caused by colonized *S.aureus*.

### 3.8. Cell viability

In order to test the biocompatibility of the various concentrations of ST loaded PLA/CS based 3D printed scaffolds, cell viability assay was performed on CCD-1072Sk human fibroblast cell line. Before performing MTT assays, brightfield images of the cells treated with PLA, PLA/CS and PLA/CS/ 1 %, 2 %, 3 % ST were taken (Fig. 11).

It was noted in 48 h that 3 % wt ST loaded scaffolds decreased cell viability to 59 % and at 72 h it was decreased to 33 %. There was no significant cell viability difference between the control and PLA/CS/ 1 % and 2 % ST at any time point (Fig. 12).

On the other hand, to visualization of cell attachment and proliferation on the 3D printed ST loaded scaffolds, the surfaces of PLA, PLA/CS, PLA/CS/1%ST and PLA/CS/2%ST samples were scanned with SEM at the end of 72 h of incubation with CCD-1072Sk human fibroblast cell line. It is clearly seen in Fig. 13 that the human fibroblast cell structure attaches to the scaffold surfaces and proliferates.

The principle of the MTT viability test is based on the mitochondrial activity of the cells to reduce 3-(4,5-dimethylthiazol-2-yl)-2,5-diphenyltetrazolium in the cell cytoplasm to formazan crystals. Therefore this assay by itself is not enough to conclude whether any early apoptotic process was initiated or not with the ST loaded scaffold treatments in the fibroblast cells. In order to test whether early or late apoptosis was induced at PLA/CS/ 1 % and 2 % ST groups Annexin V/PI double stain assay was performed. There was no significant increase between control and PLA/CS/ 1 % and 2 % ST groups in terms of early or late apoptotic cell %. However there was a significant increase at early apoptotic cells at PLA/CS/ 3 % ST group to 60.17 % compared to control group 1.08 % and also for the late apoptotic cells as well (Fig. 14).

ST loaded 3D printed scaffolds were also tested for their ability of increasing wound healing at CCD-1072Sk cells by the wound healing assay. Due to the toxicity of the 3 % ST loaded scaffolds this group was not included into the wound healing assay. First of all, the wounds were opened on human fibroblast cells for all groups and brightfield images were taken under microscope (Fig. 15, 0 h). Afterwards CCD-1072Sk

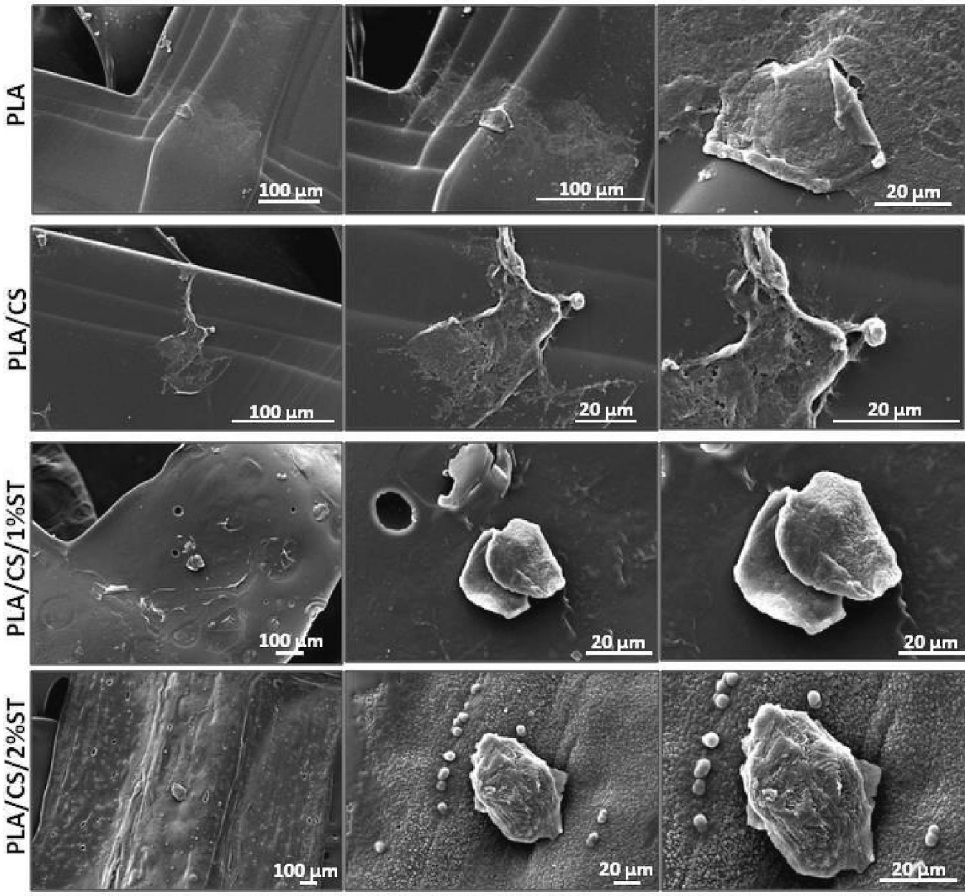


**Fig. 13.** The 3rd day high to low magnification SEM images of PLA, PLA/CS, PLA/CS/1%ST and PLA/CS/2%ST 3D scaffolds that incubated with CCD-1072Sk cells (From left to the right). Scale bars are between 100 and 20 µm related to the magnification.

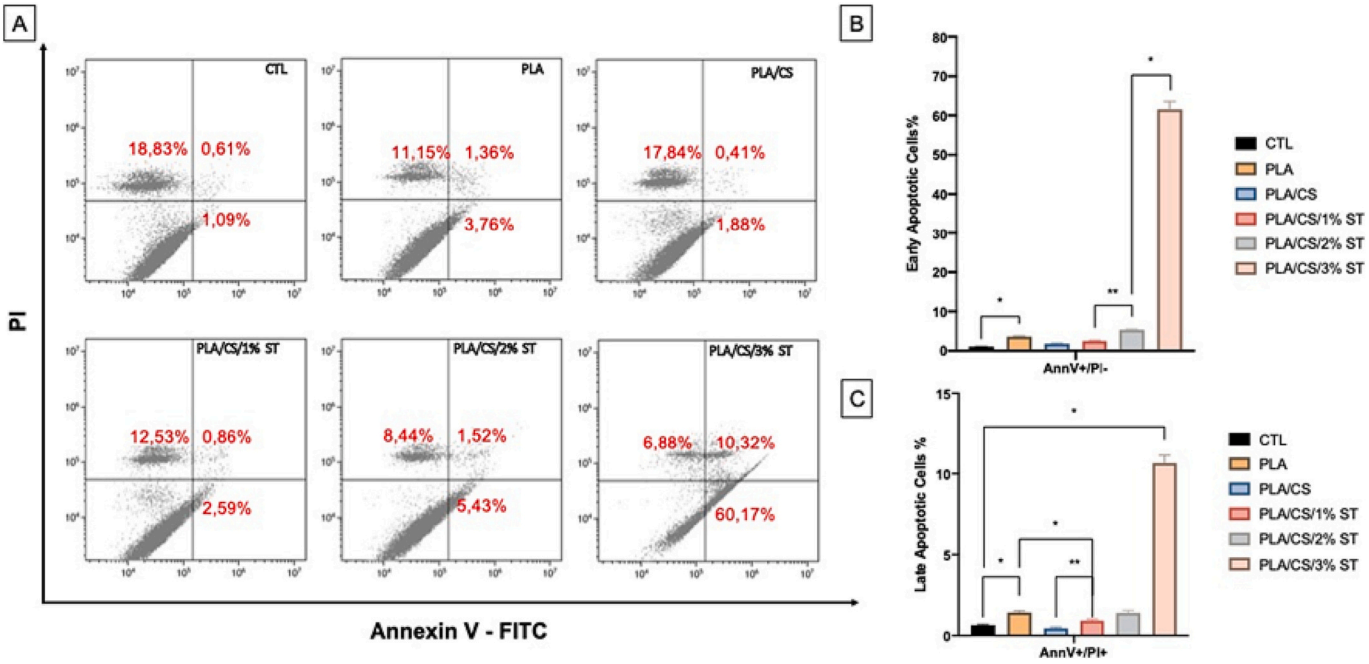


**Fig. 14.** Flow cytometry analysis of early and late apoptotic cells after 72 h of treatment with ST loaded PLA/CS scaffolds. Dot plot graphics of flow cytometry nalysis of CCD-1072Sk cells treated with PLA, PLA/CS, PLA/CS/1 %, 2 % and 3 % ST labeled with Annexian V-FITC (x-axis) and propidium iodide (y-axis). Early and late apoptotic cells were shown at the upper and lower right quadrant of each panel (a). Representative bar graph of early apoptotic cell % (b), Representative bar graph of late apoptotic cell % (c). Columns show mean values of three independent experiments (±SD). SD, standart deviation. *$p < 0,05$ and **$p < 0,005$.

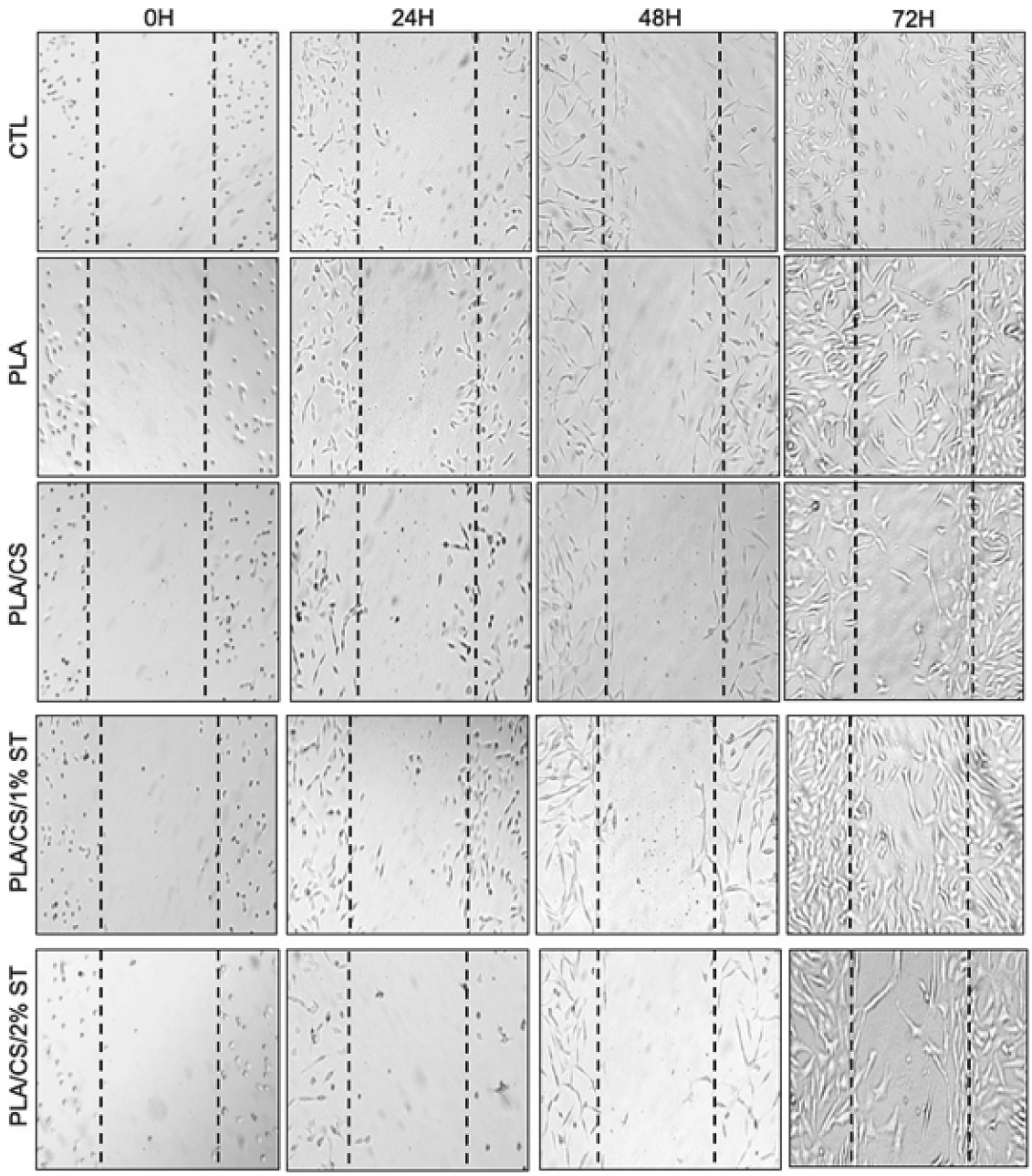


**Fig. 15.** Effects of ST loaded scaffolds on human fibroblast wound healing process. Wound healing analysis of CCD-1072Sk cells incubated with different scaffolds containing various concentrations of ST for 24, 48 and 72 h. Images were taken at 0, 24, 48 and 72 h under brightfield microscopy, 4× magnification, scale bar: 50 μm.

cells were treated with PLA, PLA/CS, PLA/CS/ 1 % and 2 % ST scaffolds for 24, 48 and 72 h. At the end of each incubation time, scaffolds were removed and brightfield images of wounds were taken at 4× magnification. Highest wound closure compared to the control group was seen on cells treated with PLA/CS/ 1 % ST for 72 h (Fig. 15). There was no significant change in terms of wound closure between control, PLA/CS and PLA/CS/ 2 % ST groups.

## 4. Conclusion

In this study, ST loaded PLA/CS scaffolds were successfully fabricated with 3D printing technology. To test the ability to accelerate the wound healing process and reduce the risk of potential infection, the PLA/CS based 3D printed scaffolds were loaded with different amounts of ST. The antimicrobial test and wound healing analysis results revealed that 1 % ST loaded PLA/CS based scaffolds exhibited a good antibacterial effect on *S. aureus* and a high wound closure effect. It has been reported in the literature that the wound closure effect is related to cell attachment and proliferation on the scaffold surface. Owing to the advantages of 3D printing technology, scaffolds with pores that provide cell attachment and proliferation have been obtained. It is seen that the average pore size of the produced PLA/CS/1%ST scaffold is <600 μm. CCD-1072Sk human fibroblast cells were observed to adhere to PLA, PLA/CS, PLA/CS/1%ST, and PLA/CS/2%ST scaffolds. Consistent with the cell viability results and SEM images, while CCD-1072Sk human fibroblast cells adhered to PLA, PLA/CS, PLA/CS/1%ST and PLA/CS/% 2ST scaffolds, no cell adhering was not seen to PLA/CS/3%ST scaffold since it was found toxic. Considering that all tests were performed with

human fibroblast cells, it can be said that 3D printed scaffolds loaded with 1 % ST could be a promising material for wound dressing applications in tissue engineering.

## CRediT authorship contribution statement

Hanife Yuksel Cakmak: Methodology, data curation. Hasan EGE: Writing- Original draft preparation, Methodology, Senanur Yilmaz: Visualization, Investigation. Gozde Enguven: Visualization, Investigation Gokhan Agturk: Conceptualization, Methodology. Fulya Dal Yontem: Conceptualization, Methodology. Abdurrahman Sarmis: Formal analysis, Methodology. Zeren Cakmak: Methodology, data curation. Oguzhan Gunduz: Project administration Zeynep Ruya Ege: Formal analysis, Supervision, Writing- Reviewing and Editing.

## Declaration of competing interest

The authors declare that they have no known competing financial interests or personal relationships that could have appeared to influence the work reported in this paper.

## Appendix A. Supplementary data

Supplementary data to this article can be found online at https://doi.org/10.1016/j.ijbiomac.2023.125835.

## References


[1] A.C.D.O. Gonzalez, Z.D.A. Andrade, T.F. Costa, A.R.A.P. Medrado, Wound healing - a literature review, An. Bras. Dermatol. 91 (5) (2016) 614.

[2] D. Atlas, IDF Diabetes Atlas, 9th edition, International Diabetes Federation, 2019. Retrieved from http://www.idf.org/about-diabetes/facts-figures.

[3] E. Eriksson, P.Y. Liu, G.S. Schultz, M.M. Martins-Green, R. Tanaka, D. Weir, G. C. Gurtner, Chronic wounds: treatment consensus, Wound Repair Regen. 30 (2) (2022) 156–171.

[4] M.A. Fonder, G.S. Lazarus, D.A. Cowan, B. Aronson-Cook, A.R. Kohli, A. J. Mamelak, Treating the chronic wound: a practical approach to the care of nonhealing wounds and wound care dressings, J. Am. Acad. Dermatol. 58 (2) (2008) 185–206.

[5] A.G. Tabriz, D. Douroumis, Recent advances in 3D printing for wound healing: a systematic review, Journal of Drug Delivery Science and Technology 74 (2022), 103564.

[6] M. Alizadehgiashi, C.R. Nemr, M. Chekini, D. Pinto Ramos, N. Mittal, S.U. Ahmed, N. Khuu, S.O. Kelley, E. Kumacheva, Multifunctional 3D-printed wound dressings, ACS Nano 15 (7) (2021) 12375–12387.

[7] M.H. Nadhif, H. Assyarify, M. Irsyad, A.R. Pramesti, M. Suhaeri, Recent advances in 3D printed wound dressings, AIP Conference Proceedings 2344 (1) (2021), 020021.

[8] R.A.A. Muzzarelli, P. Morganti, G. Morganti, P. Palombo, M. Palombo, G. Biagini, C. Muzzarelli, Chitin nanofibrils/chitosan glycolate composites as wound medicaments, Carbohydr. Polym. 70 (3) (2007) 274–284.

[9] H. Liu, C. Wang, C. Li, Y. Qin, Z. Wang, F. Yang, J. Wang, A functional chitosan-based hydrogel as a wound dressing and drug delivery system in the treatment of wound healing, RSC Adv. 8 (14) (2018) 7533–7549.

[10] W.J. Choi, K.S. Hwang, H.J. Kwon, C. Lee, C.H. Kim, T.H. Kim, S.W. Heo, J.H. Kim, J.Y. Lee, Rapid development of dual porous poly(lactic acid) foam using fused deposition modeling (FDM) 3D printing for medical scaffold application, Mater. Sci. Eng. C 110 (2020), 110693.

[11] S. Farah, D.G. Anderson, R. Langer, Physical and mechanical properties of PLA, and their functions in widespread applications — a comprehensive review, Adv. Drug Deliv. Rev. 107 (2016) 367–392.

[12] J. Domínguez-Robles, N.K. Martin, M.L. Fong, S.A. Stewart, N.J. Irwin, M.I. Rial-Hermida, R.F. Donnelly, E. Larrañeta, Antioxidant PLA composites containing lignin for 3D printing applications: a potential material for healthcare applications, Pharmaceutics 11 (4) (2019) 165.

[13] S. Calamak, M. Ermis, In situ silver nanoparticle synthesis on 3D-printed polylactic acid scaffolds for biomedical applications, J. Mater. Res. 36 (1) (2021) 166–175.

[14] I. Gurbuz, E. Yesilada, B. Demirci, E. Sezik, F. Demirci, K.H.C. Baser, Characterization of volatiles and anti-ulcerogenic effect of Turkish sweetgum balsam (Styrax liquidus), J. Ethnopharmacol. 148 (1) (2013) 332–336.

[15] O. Sağdiç, G. Özkan, M. Özcan, S. Özçelik, A study on inhibitory effects of Sığla tree (Liquidambar orientalis Mill. Var. orientalis) storax against several bacteria, Phytother. Res. 19 (6) (2005) 549–551.

[16] Topal, U., Sasaki, M., Goto, M., & Otles, S. (2009). Chemical compositions and antioxidant properties of essential oils from nine species of Turkish plants obtained by supercritical carbon dioxide extraction and steam distillation, 59(7–8), 619–634.

[17] D. Demir, S. Özdemir, S. Ceylan, M.S. Yalcin, B. Sakım, N. Bölgen, Electrospun composite nanofibers based on poly (ε-Caprolactone) and Styrax Liquidus (Liquidambar orientalis Miller) as a wound dressing: preparation, characterization, biological and Cytocompatibility results, J. Polym. Environ. 30 (6) (2022) 2462–2473.

[18] Z.R. Ege, A. Akan, F.N. Oktar, C.C. Lin, B. Karademir, O. Gunduz, Encapsulation of indocyanine green in poly (lactic acid) nanofibers for using as a nanoprobe in biomedical diagnostics, Mater. Lett. 228 (2018) 148–151.

[19] E. Ilhan, S. Cesur, E. Guler, F. Topal, D. Albayrak, M.M. Guncu, O. Gunduz, Development of Satureja cuneifolia-loaded sodium alginate/polyethylene glycol scaffolds produced by 3D-printing technology as a diabetic wound dressing material, Int. J. Biol. Macromol. 161 (2020) 1040–1054.

[20] R. Hosseinzadeh, B. Mirani, E. Pagan, S. Mirzaaghaei, A. Nasimian, P. Kawalec, M. Akbari, A drug-eluting 3D-printed mesh (GlioMesh) for management of glioblastoma, Advanced Therapeutics 2 (11) (2019) 1900113.

[21] E. Altun, M.O. Aydogdu, F. Koç, O. Kutlu, D. Gozuacik, S. Yucel, O. Gunduz, Amoxicillin loaded hollow microparticles in the treatment of osteomyelitis disease using single-nozzle electrospinning, BioNanoScience 8 (3) (2018) 790–801.

[22] The European Committee on Antimicrobial Susceptibility Testing. Breakpoint tables for interpretation of MICs and zone diameters, Eur. Comm. Antimicrob. Susceptibility Testing. Version 12.0, http://www.eucast.org, (accessed 13 March) (2022).

[23] M. Taghizadeh, A. Taghizadeh, M.K. Yazdi, P. Zarrintaj, F.J. Stadler, J.D. Ramsey, U.S. Schubert, Chitosan-based inks for 3D printing and bioprinting, Green Chem. 24 (1) (2022) 62–101.

[24] S. Singh, G. Singh, C. Prakash, S. Ramakrishna, L. Lamberti, C.I. Pruncu, 3D printed biodegradable composites: an insight into mechanical properties of PLA/chitosan scaffold, Polym. Test. 89 (2020), 106722.

[25] Y. Dong, P. Li, C.B. Chen, Z.H. Wang, P. Ma, G.Q. Chen, The improvement of fibroblast growth on hydrophobic biopolyesters by coating with polyhydroxyalkanoate granule binding protein PhaP fused with cell adhesion motif RGD, Biomaterials 31 (34) (2010) 8921–8930.

[26] C.R. Almeida, T. Serra, M.I. Oliveira, J.A. Planell, M.A. Barbosa, M. Navarro, Impact of 3D printed PLA-and chitosan-based scaffolds on human monocyte/macrophage responses: unraveling the effect of 3-D structures on inflammation, Acta Biomater. 10 (2) (2014) 613–622.

[27] X. Zhao, Y. Liang, B. Guo, Z. Yin, D. Zhu, Y. Han, Injectable dry cryogels with excellent blood-sucking expansion and blood clotting to cease hemorrhage for lethal deep-wounds, coagulopathy and tissue regeneration, Chem. Eng. J. 403 (2021), 126329.

[28] L. Elviri, R. Foresti, C. Bergonzi, F. Zimetti, C. Marchi, A. Bianchera, R. Bettini, Highly defined 3D printed chitosan scaffolds featuring improved cell growth, Biomed. Mater. 12 (4) (2017), 045009.

[29] M. Guvendiren, J. Molde, R.M. Soares, J. Kohn, Designing biomaterials for 3D printing, ACS Biomaterials Science & Engineering 2 (10) (2016) 1679–1693.

[30] S. Ulag, E. Ilhan, A. Sahin, B.K. Yilmaz, N. Ekren, O. Kilic, O. Gunduz, 3D printed artificial cornea for corneal stromal transplantation, Eur. Polym. J. 133 (2020), 109744.

[31] D. Demir, S. Özdemir, S. Gonca, N. Bölgen, Novel styrax liquidus loaded chitosan/polyvinyl alcohol cryogels with antioxidant and antimicrobial properties, J. Appl. Polym. Sci. 139 (17) (2022) 52033.

[32] R. Wongkanya, V. Teeranachaideekul, A. Makarasen, P. Chuysinuan, P. Yingyuad, P. Nooeaid, D. Dechtrirat, Electrospun poly (lactic acid) nanofiber mats for controlled transdermal delivery of essential oil from Zingiber cassumunar Roxb, Materials Research Express 7 (5) (2020), 055305.

[33] T.T.T. Nguyen, O.H. Chung, J.S. Park, Coaxial electrospun poly (lactic acid)/chitosan (core/shell) composite nanofibers and their antibacterial activity, Carbohydr. Polym. 86 (4) (2011) 1799–1806.

[34] P. Wen, D.H. Zhu, K. Feng, F.J. Liu, W.Y. Lou, N. Li, H. Wu, Fabrication of electrospun polylactic acid nanofilm incorporating cinnamon essential oil/β-cyclodextrin inclusion complex for antimicrobial packaging, Food Chem. 196 (2016) 996–1004.

[35] K. Nejati-Koshki, Y. Pilehvar-Soltanahmadi, E. Alizadeh, A. Ebrahimi-Kalan, Y. Mortazavi, N. Zarghami, Development of emu oil-loaded PCL/collagen bioactive nanofibers for proliferation and stemness preservation of human adipose-derived stem cells: possible application in regenerative medicine, Drug Dev. Ind. Pharm. 43 (12) (2017) 1978–1988.

[36] H. Adeli, M.T. Khorasani, M. Parvazinia, Wound dressing based on electrospun PVA/chitosan/starch nanofibrous mats: fabrication, antibacterial and cytocompatibility evaluation and in vitro healing assay, Int. J. Biol. Macromol. 122 (2019) 238–254.

[37] H. Donya, R. Darwesh, M.K. Ahmed, Morphological features and mechanical properties of nanofibers scaffolds of polylactic acid modified with hydroxyapatite/CdSe for wound healing applications, Int. J. Biol. Macromol. 186 (2021) 897–908.

[38] S. Saberianpour, M. Heidarzadeh, M.H. Geranmayeh, H. Hosseinkhani, R. Rahbarghazi, M. Nouri, Tissue engineering strategies for the induction of angiogenesis using biomaterials, J. Biol. Eng. 12 (1) (2018) 1–15.

[39] Y. Wang, L. Sun, Z. Mei, F. Zhang, M. He, C. Fletcher, P. Liu, 3D printed biodegradable implants as an individualized drug delivery system for local chemotherapy of osteosarcoma, Mater. Des. 186 (2020), 108336.

[40] Shan Liu, Shuhao Qin, Min He, Dengfeng Zhou, Qingdong Qin, Hao Wang, Current applications of poly(lactic acid) composites in tissue engineering and drug delivery, Compos. Part B: Engineering 199 (2020) 108238.

[41] P. Kowalczyk, P. Trzaskowska, I. Łojszczyk, R. Podgórski, T. Ciach, Production of 3D printed polylactide scaffolds with surface grafted hydrogel coatings, Colloids Surf. B: Biointerfaces 179 (2019) 136–142.

[42] N. Charernsriwilaiwat, T. Rojanarata, T. Ngawhirunpat, M. Sukma, P. Opanasopit, Electrospun chitosan-based nanofiber mats loaded with Garcinia mangostana extracts, Int. J. Pharm. 452 (1–2) (2013) 333–343.
[43] H.A. Merchant, H.M. Shoaib, J. Tazeen, R.I. Yousuf, Once-daily tablet formulation and in vitro release evaluation of cefpodoxime using hydroxypropyl methylcellulose: a technical note, AAPS PharmSciTech 7 (3) (2006) E178–E183.
[44] M. Hormozi, R. Assaei, M.B. Boroujeni, The effect of aloe vera on the expression of wound healing factors (TGFβ1 and bFGF) in mouse embryonic fibroblast cell: in vitro study, Biomed. Pharmacother. 88 (2017) 610–616.
[45] A.I. Prisăcaru, C.V. Andriţoiu, C. Andriescu, E.C. Hăvârneanu, M. Popa, A. G. Motoc, A. Sava, Evaluation of the wound-healing effect of a novel Hypericum perforatum ointment in skin injury, Romanian J. Morphol. Embryol. 54 (4) (2013) 1053–1059.
[46] G. Okmen, O. Turkcan, O. Ceylan, G. Gork, The antimicrobial activity of Liquidambar orientalis mill. Against food pathogens and antioxidant capacity of leaf extracts, Afr J Tradit Complement Altern Med. 11 (5) (2014) 28–32 (Published 2014 Aug 23).
[47] O. Sağdiç, G. Ozkan, M. Ozcan, S. Ozçelik, A study on inhibitory effects of Siğla tree (Liquidambar orientalis Mill. Var. orientalis) storax against several bacteria, Phytother. Res. 19 (6) (2005) 549–551.
[48] T.J. Hatlen, L.G. Miller, Staphylococcal skin and soft tissue infections, Infect. Dis. Clin. N. Am. 35 (1) (2021) 81–105.
[49] S. Roy, S. Santra, A. Das, S. Dixith, M. Sinha, S. Ghatak, C.K. Sen, Staphylococcus aureus biofilm infection compromises wound healing by causing deficiencies in granulation tissue collagen, Ann. Surg. 271 (6) (2020) 1174.
[50] EUCAST, European committee on antimicrobial susceptibility testing, Routine and extended internal quality control for MIC determination and disk diffusion as recommended by EUCAST Version 12.0, valid from 2022-01-01.
[51] J. Wróbel, H. Tomczak, D. Janerowicz, M. Czarnecka-Operacz, Skin and nasal vestibule colonisation by Staphylococcus aureus and its susceptibility to drugs in atopic dermatitis patients, Annals of Agricultural and Environmental Medicine 25 (2) (2018).
[52] K. Shettigar, T.S. Murali, Virulence factors and clonal diversity of Staphylococcus aureus in colonization and wound infection with emphasis on diabetic foot infection, Eur. J. Clin. Microbiol. Infect. Dis. 39 (2020) 2235–2246.
[53] R. Serra, R. Grande, L. Butrico, A. Rossi, U.F. Settimio, B. Caroleo, S. De Franciscis, Chronic wound infections: the role of Pseudomonas aeruginosa and Staphylococcus aureus, Expert Rev. Anti-Infect. Ther. 13 (5) (2015) 605–613.
[54] M. Fayolle, M. Morsli, A. Gelis, M. Chateauraynaud, A. Yahiaoui-Martinez, A. Sotto, C. Dunyach-Remy, The persistence of Staphylococcus aureus in pressure ulcers: a colonising role, Genes 12 (12) (2021) 1883.
[55] M. Palomar, J. Insausti, P. Olaechea, E. Cerdá, M.V. De la Torre, Staphylococcus aureus nosocomial infections in critically ill patients admitted in intensive care units, Medicina Clinica 126 (17) (2006) 641–646.
[56] N. Sharma, A.K. Chhillar, S. Dahiya, A. Punia, P. Choudhary, P. Gulia, M. Dangi, Chemotherapeutic strategies for combating Staphylococcus aureus infections, Mini Reviews in Medicinal Chemistry 22 (1) (2022) 26–42.